Solving the Reservoir Ambiguity Using the Combination of PVT, Well Test, Petrophysical and Geophysical Data

Edwin R. Gonzalez[1], Heri Tanjung[1], Han N. Tran[1], Omar Al-Shaiji[1], and Abdullah A. Al-Fawwaz[1]

Search and Discovery Article #42603 (2025)**
Posted November 8, 2025

*Adapted from extended abstract based on oral presentation given at AAPG International Conference and Exhibition (ICE) Rio de Janeiro, 30 September - 3 October, 2025.
 DOI:10.1306/42603Tanjung2025

[1]Aramco Gulf Operation Company, Khafji, Eastern Province, Saudi Arabia

Abstract

The field is in the offshore Arabian Gulf, mainly associated with basement-involved wrench-dominated strike slip faulting system. This typical kinematics created paths for hydrocarbon migration and accumulation into the reservoirs. Several exploration and appraisal wells have been drilled to confirm the structure and the properties of the main Lower Cretaceous Carbonate reservoir, which contains gascondensate, oil rim and water. One of the challenges was to distinguish the exact contact between gas-condensate and oil rim, in which most of the well log data cannot distinguish the contact in a straightforward manner. For example, there is no clear separation between density and neutron log although well testing result shows the change in formation fluid. In addition, the prominent gas condensate is only found in this particular part of the reservoir, not even in the shallower ones, which raised the question of its origin. Furthermore, the cuttings over gas reservoir interval always show oil stains which complicates the interpretation.

To solve this matter, an integrated study utilizing PVT, well test, well log, mud-log and seismic data was performed. This paper shows the approach using the compositional grading simulation (CGS) from PVT data to obtain robust fluid contact before finally being checked against the well testing data. Petrophysical analysis was performed using standard triple combo logs combined with nuclear magnetic resonance (NMR) log which was validated by available core data. 3D seismic data structural interpretation was done to confirm the migration path of the hydrocarbon inside the field.

Fluid property analysis showed compositional grading as the depth increases with abrupt change of API from around 50 to 35 at a certain depth, which not only indicating the fluid contact but also giving the indication of the original oil replacement in the reservoir by gas condensate. This approach has also solved the ambiguity of well test results in distinguishing oil associated with gas condensate and oil from the oil rim. The comparison between oil saturation from core data and irreducible fluid saturation from NMR strengthened the postulate of possible initial oil replacement by gas condensate. These findings can explain the occurrence of oil stains on cuttings data, which indicates that initial fluid in the reservoir was oil. 3D seismic data confirmed that basement-involved strike slips faults creating the paths for the gas migration into the reservoir.

The study has not only shed some light in determining the fluid contact in a more accurate manner, which was not possible using only conventional well log and well test data, but also providing proof of oil replacement by gas condensate in the reservoir. These findings are also in-line with the current understanding of strike-slip tectonic regime which allows the accumulation of gas condensate in this reservoir.

Background

The study focusses on the Lower Cretaceous carbonates reservoir which was deposited on open platforms within intra-shelf basins of the Arabian plate that was surrounded from the north, east, and south by passive margins with Neo-Tethys (Ziegler, 2001). This interval is characterized by moderately high, but falling eustatic sea level (Haq et al., 1988). The eastern shelf platform of the Arabian Plate, which includes the study area was covered by shallow-water carbonates. The general overview of the stratigraphic column based on Sharland et al. (2002) is depicted in Fig. 1. Due to company policies, it is not possible to display the exact location of the field, name of formation, actual depth interval and certain log scale.

Reservoir Ambiguities

Fig. 2 shows the correlation of six representative wells for this study, in which no prominent density-neutron separation can be observed over the gas condensate interval. Both density and neutron logs are pretty much overlying each other across the whole reservoir as they are displayed on limestone compatible scale. There is some visible decrease of resistivity reading as they enter the liquid interval although they are also affected by low porosity zone. These pose some uncertainties to determine the fluid contact only based on the log response. Thus, pressure gradient and fluid sampling from downhole formation tester are essential to determine the fluid contact. The available PVT information depicts two distinct values of API oil range: those around 45 and those around 35, which suggests two different types of oil. Oil with API around 45 is associated with gas-condensate and those around 35 API are associated with the oil rim.

In-situ oil saturation from the core data which are shown on the seventh track in each well plot (Fig. 2) shows remaining oil saturation even in the wet well (B) and upper part of the reservoir in several wells (A, C, F). The eighth track shows irreducible fluid saturation (black shading) which is computed from the comparison between total porosity and NMR bound fluid volume displayed on the ninth track. The irreducible fluid saturation from NMR corresponds to both residual/immobile oil and irreducible water. In the porous zone where irreducible water should be relatively less compared to those in tight zone; the increase of irreducible fluid saturation might be related to increase of residual/immobile oil. Furthermore, the mudlog also describes the occurrence of oil stain over the gas condensate interval.

Hence, these are two main ambiguities which will be discussed in this paper; those related to fluid contact and the previously overlooked residual oil. The next part of this paper will describe the findings in each well in more detail to address the aforementioned reservoir ambiguities. For the sake of practicality, all well plots displayed in Fig. 4 to Fig. 10 are using same track order as depicted in Fig. 3.

Well A

The available logs in well A are described in Fig. 4. There is no distinctive reading from the logs to tell the exact gas-oil contact in this well.

There is no visible density-neutron separation to enable gas and liquid recognition. Resistivity reading is also affected by tight reservoir. Sometimes, the crossover of deep and flushed resistivity can be an indicator of the change from gas condensate to oil in which the flushed resistivity reads significantly lower than the deep resistivity. In this well, the separation can be observed from the top of reservoir to X475 and around X560 - X590. The fluid contact in this well is defined based on available pressure gradient from the well test, flow from production logging tool (PLT) and oil API from PVT data which is approximately at around X585. Note that two PVT data of oil sample show 46 deg API which is associated with the gas condensate. However, there is some doubt about the fluid at around X525, in which deep and flushed resistivity are overlaying each other with significant increase of in-situ oil saturation from the core and increase in immobile fluid saturation from NMR. Unfortunately, the fluid sample is not conclusive at this depth.

This well exhibits an increase of in-situ oil saturation from the core, especially around the top of the condensate gas reservoir. There is also some residual oil in the middle and lower part of the gas-condensate interval. The irreducible fluid saturation from NMR (black shading) which is derived from the ratio of bound fluid volume from NMR against the total porosity, indicates significant presence of immobile fluid. Apparently, the remaining oil saturation observed from the core data is not movable at all.

The occurrence of immobile oil over the gas condensate zone leads to the interpretation that the reservoir was initially filled with oil before lighter hydrocarbon migration into this reservoir.

Well B

The available logs in well B are described in Fig. 5. This is a wet well as confirmed from DST data and relatively low resistivity reading. There is no significant crossover between flushed and deep resistivity to indicate the fluid change from gas condensate to oil. By far, well B is the deepest well penetrating this particular reservoir in this field. The saturation at around X750-X800 is not valid as the openhole logs such as density are heavily affected by borehole rugosity.

The in-situ oil saturation reading from the core exhibits an increase towards the top of the reservoir. Unfortunately, there is no NMR log available in this well. The occurrence of immobile oil over the wet zone of this reservoir leads to the interpretation that the reservoir was initially filled with oil.

Well C

The available logs in well C are described in Fig. 6. There is no visible density-neutron separation to enable gas and liquid recognition. Resistivity reading is also affected by tight reservoir although the separation between flushed and deep resistivity above X290 indicates the gas condensate occurrence. There is no pressure gradient data available in this well. Based on the resistivity separation and DST data, the contact is estimated to be at X290. PVT data of oil samples around X400 shows 33.2 deg API which is associated with the oil rim.

In-situ oil saturation from the core over gas condensate interval at around X230 shows the presence of residual/immobile oil, while those around X350 and X450 are quite matching with the saturation computed from the logs. The occurrence of immobile oil over the gas condensate zone leads to the interpretation that the reservoir was initially filled with oil before lighter hydrocarbon migration into this reservoir.

Well D

The available logs in well D are described in Fig. 7. There is no visible density-neutron separation to enable gas and liquid recognition. Resistivity reading is affected by tight reservoir although the separation between flushed and deep resistivity above X315 indicates the gas condensate occurrence, which is also supported by pressure gradient from well testing data. However, PLT flow profile shows the gas contribution starting from around X270. Based on the resistivity separation and pressure gradient data, the contact is estimated to be at X315.

The irreducible fluid saturation from NMR (black shading) which is derived from the ratio of bound fluid volume from NMR against the total porosity, indicates an increase of immobile fluid towards the top of reservoir over the porous zone. The overall reading of immobile fluid saturation is not as high as those in well A, both in gas condensate and oil interval. Although there is no available in-situ oil saturation from the core in this well, the increase of immobile fluid saturation towards the top of reservoir might be associated with the increase of residual oil, despite the low porosity effect.

Well E

The available logs in well E are described in Fig. 8 and Fig. 9. There is no visible density-neutron separation to enable gas and liquid recognition. Resistivity separation between flushed and deep resistivity doesn't really indicate the gas-oil contact in this well, although the deep resistivity is decreasing below X470. The pressure gradient data shows that the contact is estimated to be at X470. The fluid sampling result supports this estimated contact as gas samples were obtained above X470, and oil samples were obtained slightly below X470. The oil samples below X470 read at around 35 deg API which are associated with oil rim.

An isothermal compositional grading simulation (CGS) as described by Høier and Whitson (2001) and Whitson et al., (1994) was performed in this well to give a better idea on the possible fluid contact which is based on the compositional change analysis. Compositional gradient is a phenomenon that occurs when the chemical potential and gravitational potential equilibrate, resulting in a variation in the composition versus depth. Gas-oil contact from compositional grading simulation is the depth where the fluid system changes from a mixture with bubble point to a mixture with dew point. A gas-oil contact is seen at a depth at which the saturation pressure and reservoir pressure coincide. The CGS result shows saturated condition, in which the GOC gas is in thermodynamic equilibrium with GOC oil and reservoir pressure equals the bubble point of the GOC oil which equals the dew point of the GOC gas.

The compositional grading simulation result in well E shows similar gas-oil contact at around X470 as shown in Fig. 8 (b), which is inline with gas-oil contact observation from pressure gradient and fluid sampling. In addition, the gas chromatogram from mudlogs also shows a notable decrease below X470 as shown in Fig. 8 (c).

The irreducible fluid saturation from NMR (black shading) shown in Fig. 8 (a), which is derived from the ratio of bound fluid volume from

NMR against the total porosity, indicates a significant increase of immobile fluid towards the bottom of reservoir over the porous zone below the estimated gas-oil contact at X470. Unfortunately, there was a stuck fish at around X200-X315 which disallowed the NMR data acquisition over this interval. The overall reading of immobile fluid saturation is not as high as those in well A, except below X470. Although there is no available in-situ oil saturation from the core in this well, the significant increase of immobile fluid saturation towards the bottom of the reservoir might be associated with the significant increase of residual oil in this interval.

With similar approach, the compositional grading simulation was also performed to check the unusual response of gas chromatogram behavior at around X285 which shows significant drop of C1 in a way that crossover between C1 and C2 is visible as shown in Fig. 9 (c). The result of the compositional grading simulation shows unexpected gas-oil contact at around X285 as shown in Fig. 9 (b), which matches the strange phenomenon of C1 from gas chromatogram. Note that standard open-hole logs don't show any indication of gasoil contact around this interval previously (Fig. 8 (a)). Based on this result, it is interpreted to have possible oil accumulation at around X285-X320 just above the tight zone of X320-X345 (Fig. 9 (a)). Unfortunately, neither oil saturation from core nor NMR log is available over this interval to investigate further on the fluid mobility.

This case shows the advantage of performing the compositional grading simulation in gas condensate reservoir to solve the ambiguity especially in identifying the fluid contact.

Well F

The available logs in well F are described in Fig. 10 (a). There is no visible density-neutron separation to enable gas and liquid recognition. Resistivity separation between flushed and deep resistivity indicates possible gas-oil contact at around X450. The pressure gradient data shows that the contact is estimated to be at X445. The fluid sampling result supports this estimated contact as gas samples were obtained above X415, and oil samples were obtained slightly below X455. There is a significant contrast in term of API degree between oil sample around X415 and oil sample around X455. The oil sample with 47.5 deg API is associated with gas condensate, while those with 34.6 is associated with oil rim. These observations satisfy the estimated gas-oil contact at around X445.

Similar isothermal compositional grading simulation (CGS) as described by Høier and Whitson (2001) was also performed in this well just like in well E to give a better idea on the possible fluid contact which is based on the compositional change analysis (Fig. 10 (b)). The CGS result shows saturated condition which also satisfies the gas-oil contact interpretation at around X445. In addition, the gas chromatogram from mudlogs also shows a notable decrease below X445 as shown in Fig. 10 (c).

The irreducible fluid saturation from NMR (black shading) shown in Fig. 10 (a), which is derived from the ratio of bound fluid volume from NMR against the total porosity, indicates a significant increase of immobile fluid at around X500 which is associated with tar mat. The overall reading of immobile fluid saturation is not as high as those in well A, except on the tar mat interval. In-situ oil saturation from the core in this well shows some increase which also coincides with the increase of immobile fluid saturation from NMR at around X200, which might be associated with the increase of residual oil in this gas-condensate interval.

Observation

The in-situ oil saturation from core data which shows some residual oil in gas condensate and wet zone might be an indicative that the reservoir was initially oil reservoir. High immobile fluid saturation from NMR which is the sum of immobile oil and irreducible water can give some idea on the occurrence of residual oil in the porous interval over the gas condensate reservoir.

The standard open-hole logs might struggle to clearly define the fluid contact, especially between gas condensate and oil in this reservoir. The combination approach utilizing pressure gradient from well testing, PVT data from fluid sampling and PLT are very useful to determine the contact in a more accurate manner. In addition, the compositional grading simulation (CGS) is also helpful to determine the contact between gas condensate and oil. The CGS has also revealed the unexpected gas-oil contact over the gas condensate zone at X285 in well E just above the tight zone. This finding opens the possibility of having similar case of possibly "trapped oil" at X525 in well A.

This unexpected gas-oil contact over gas condensate zone, possible "trapped oil" above gas-oil contact, combined with the residual oil information from core and NMR might be the manifestation of the leftover oil before the migration of gas into this reservoir replacing some portion of initial oil and turning it into gas condensate reservoir.

Postulate

Based on the aforementioned observations, it is postulated that the gas condensate reservoir was initially oil reservoir. Taking the analogue from the Baiyun Depression which was described by Wang et al. (2022), continuous gas charging into this reservoir has increased the gas-oil ratio and dissolving the light oil in the gas. With the increase in pressure and temperature due to burial, the oil reservoir eventually turned into a gas condensate reservoir. Fig. 11 illustrates the process of turning the oil reservoir into gas condensate reservoir.

Although there is not much study about geochemistry in this field at the moment, there are representative rock-eval pyrolysis samples from Upper Jurassic limestone formation as depicted in Fig. 12 and Fig. 13 to strengthen this postulate. Fig. 12 (a) shows the oil-prone type-II kerogen source rock based on oxygen index and hydrogen index from rock-eval pyrolysis with maturity within oil generating window based on Tmax and hydrogen index plot from rock-eval pyrolysis (Fig. 12 (b)). Fig. 13 (a) shows the gas-prone type-III kerogen source rock based on oxygen index and hydrogen index from rock-eval pyrolysis with maturity reaching gas generating window based on Tmax and hydrogen index plot from rock-eval pyrolysis (Fig. 13 (b)).

The seismic interpretation of this field depicts the occurrence of flower structure which is a possible conduit for hydrocarbon migration in this field. The source rock interval is shown in red dash line on Fig. 14, while the green dotted line indicates the reservoir interval.

Implications

These findings and postulates provide valuable insight into the subsequent process of static and dynamic reservoir modelling of the reservoir, which might account for detrimental technical consequences if neglected such as oil in-place overestimation, gas in-place underestimation, etc., as described by Igwe et al., (2020). Furthermore, the acquisition of complete core data along with advanced log such as NMR which cover the whole gas condensate and oil rim interval are important for future drilling in this field. Last but not least, well testing and fluid sampling are also paramount to shed more light on this relatively low contrast gas condensate reservoir.

References

Haq, B.U., Hardenbol, J., and Vail, P.R., 1988, Mesozoic and Cenozoic Chronostratigraphy and Cycles of Sea-level Change. In: Wilgus et al. (Eds.), Sea-level Changes: An Integrated Approach, Society Economic Paleontologists Mineralogists, Special Publication No. 42, pp. 71-108.

Høier, L., and Whitson, C.H., 2001, Compositional Grading—Theory and Practice, SPE Res Eval & Eng 4: 525-535.

Igwe, I., Gholinezhad, J., Sayed, M.G.H., and Ogbuagu, F., 2020, Technical Implication of Neglecting Compositional Grading Effects in Petroleum Reservoir Simulation Models, Journal of Energy and Fuels 34 (2): 1467-1481.

Sharland, P.R., Archer, R., Casey, D.M., Davis, R.B., Hall, S.H., Howard, A.P., Horbury, A.D., and Simmons, M.D., 2002, Arabian Plate Sequence Stratigraphy, GeoArabia, Spec. Publ. 2, 372p.

Wang, C., Zeng, J., Zhang, G., and Yin, X., 2022, Formation Processes of Gas Condensate Reservoirs in The Baiyun Depression: Insights from Geochemical Analysis and Basin Modelling, Journal of Natural Gas Science and Engineering, Vol. 100.

Whitson, C.H., Trondheim, U., and Belery, P., 1994, Compositional Gradients in Petroleum Reservoirs, Paper presented at University of Tulsa Centennial Petroleum Engineering Symposium, Tulsa, USA, 29-31 August.

Ziegler, M.A., 2001, Late Permian to Holocene Paleofacies Evolution of the Arabian Plate and Its Hydrocarbon Occurrences, GeoArabia, 8 (2): 445-504.

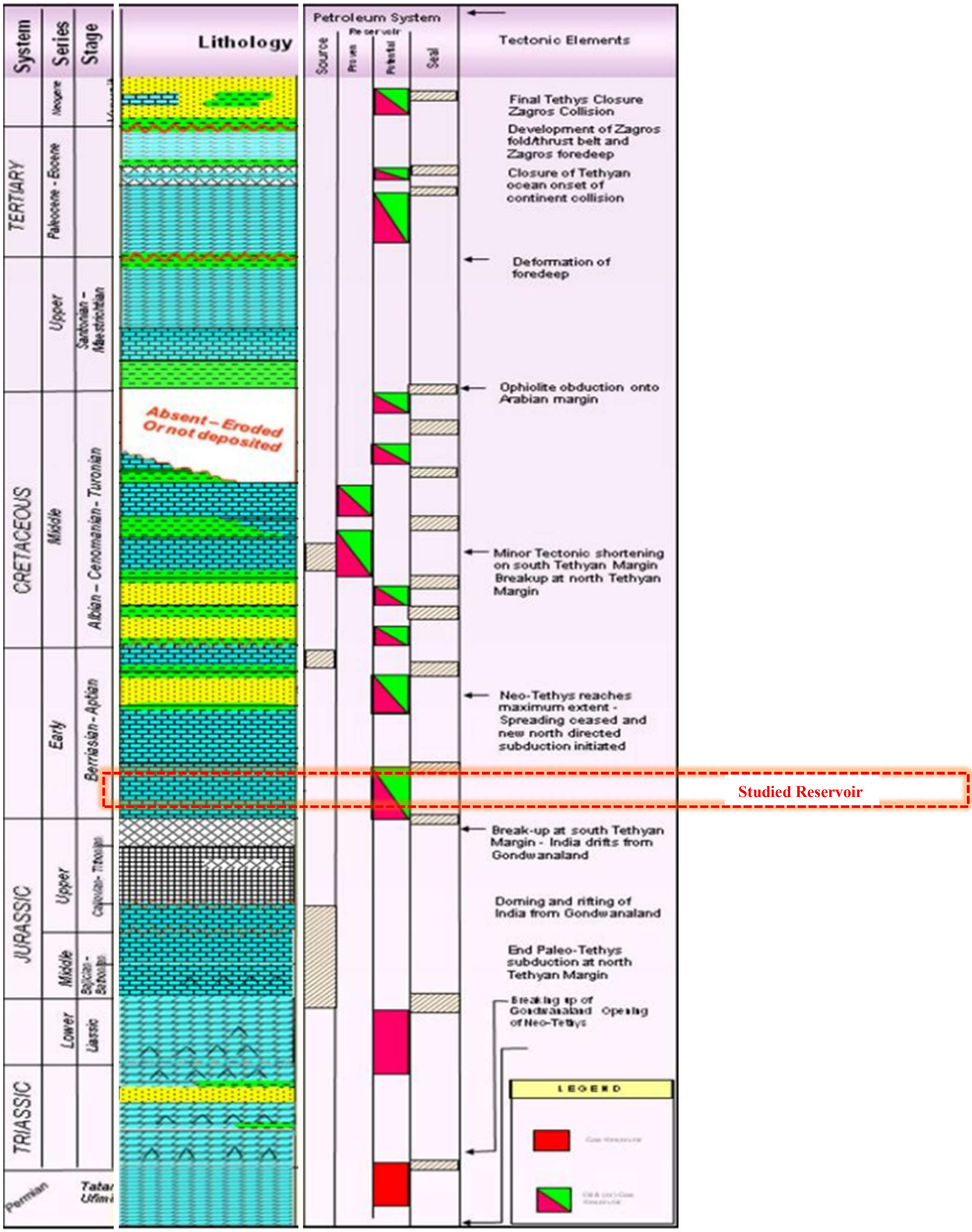

Figure 1. Stratigraphic succession of the studied reservoir (modified after Sharland et al., 2002).

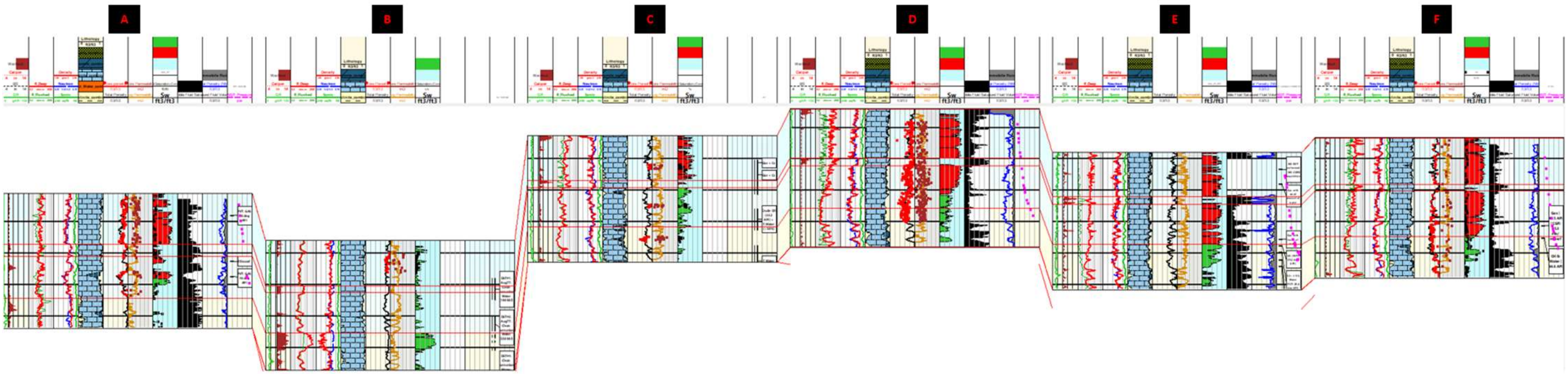

Figure 2. The correlation of six representative wells is shown here. The first track from the left of each wells contains caliper and GR reading; the second track contains resistivity logs; the third track contains density-neutron-sonic readings; the fourth track shows the lithology volume; the fifth track shows the computed porosity based on the logs and core porosity; the sixth track shows the computed permeability based on the logs and core permeability; the seventh track shows the saturation from the logs (Sw) along with in-situ oil saturation reading from the core; the eighth track contains the irreducible fluid saturation based on NMR log; the ninth track shows the comparison between total porosity and bound fluid volume from NMR log; and tenth track shows the pressure gradient from downhole formation tester.

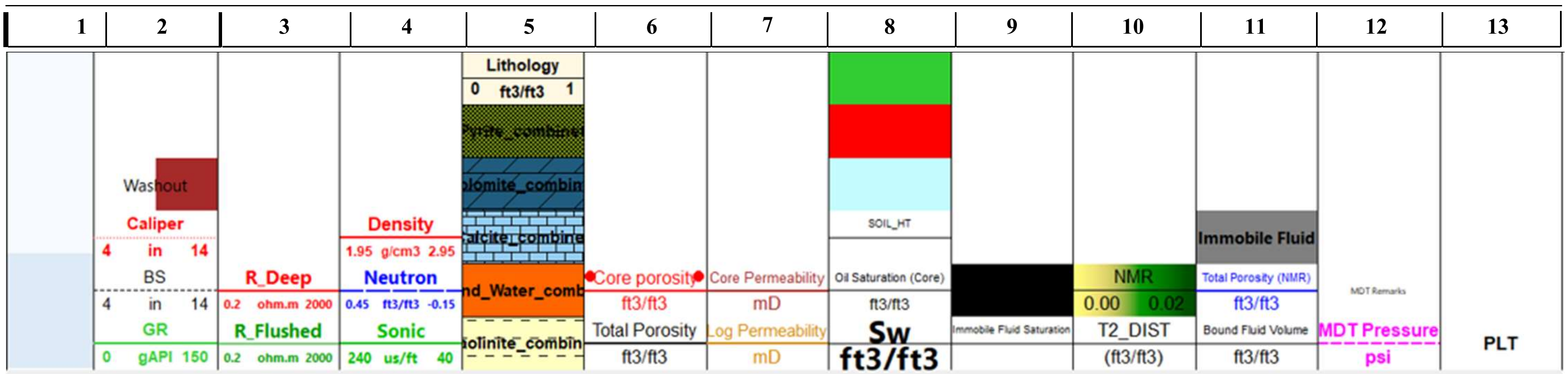

Figure 3. The uniform log header for all well plots. Track 1—Dummy Depth, Track 2—GR, Caliper, Track 3—Resistivity, Track 4—Density-Neutron- Sonic, Track 5—Lithology Volume, Track 6—Total and Core Porosity, Track 7—Permeability from Log and Core, Track 8—Sw from log and So from core, Track 9—Immobile Fluid Saturation from NMR, Track 10—T2 Distribution from NMR, Track 11—Total Porosity and Bound Fluid Volume from NMR, Track 12—Pressure from Well Test along with Fluid Information, Track 13—PLT profile.

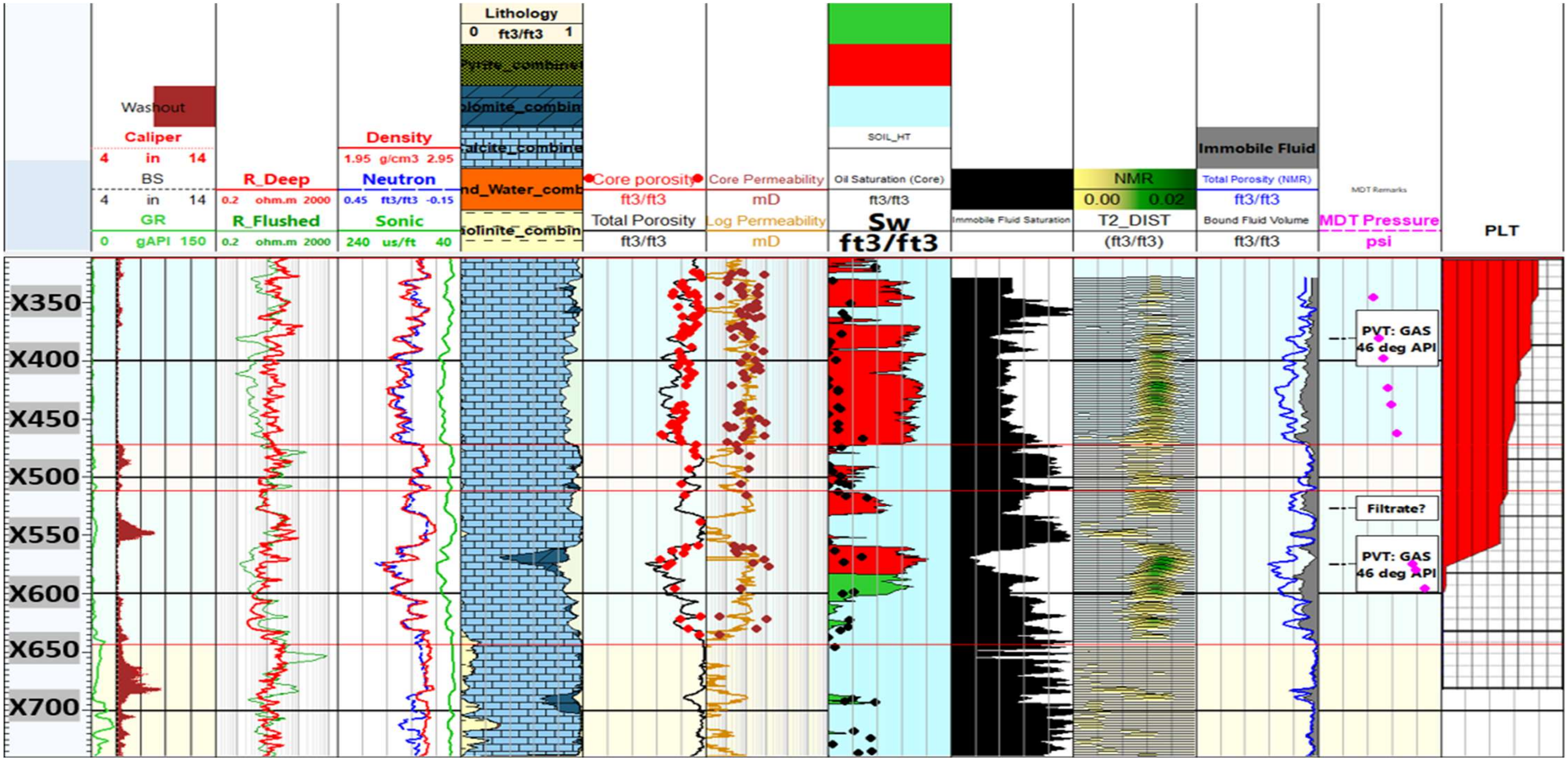

Figure 4. The plot shows available log data in well A. The immobile fluid saturation on track 9 shows the highest reading among the observed six wells in this study. In-situ oil saturation from core on track 8 shows residual oil over gas condensate zone. The gas-oil contact is determined based on pressure gradient, PLT and PVT data. Note that PVT data shows 46 deg API which corresponds to gas condensate occurrence.

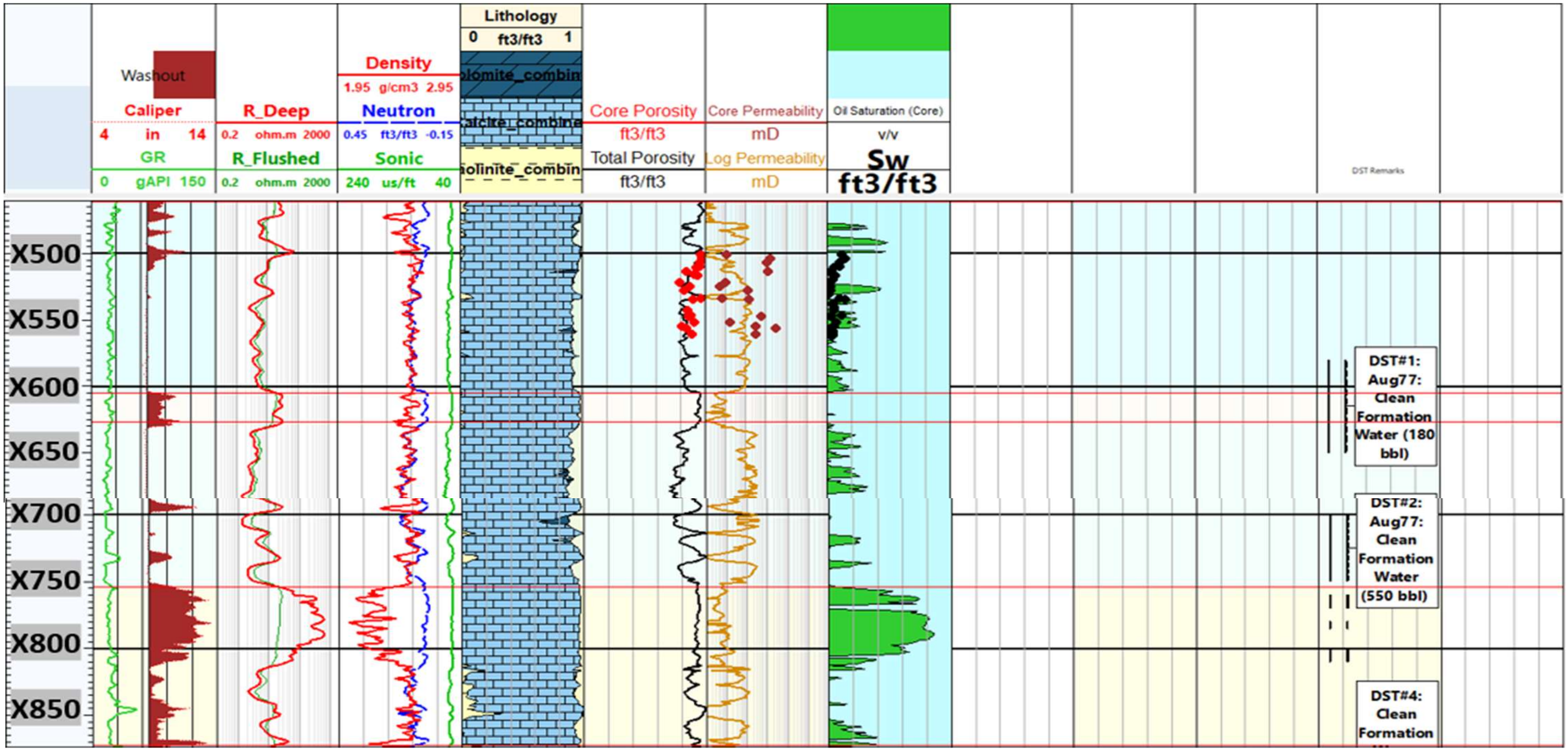

Figure 5. The plot shows available log data in well B. The saturation around X750-X800 is not valid due to the washout effect.

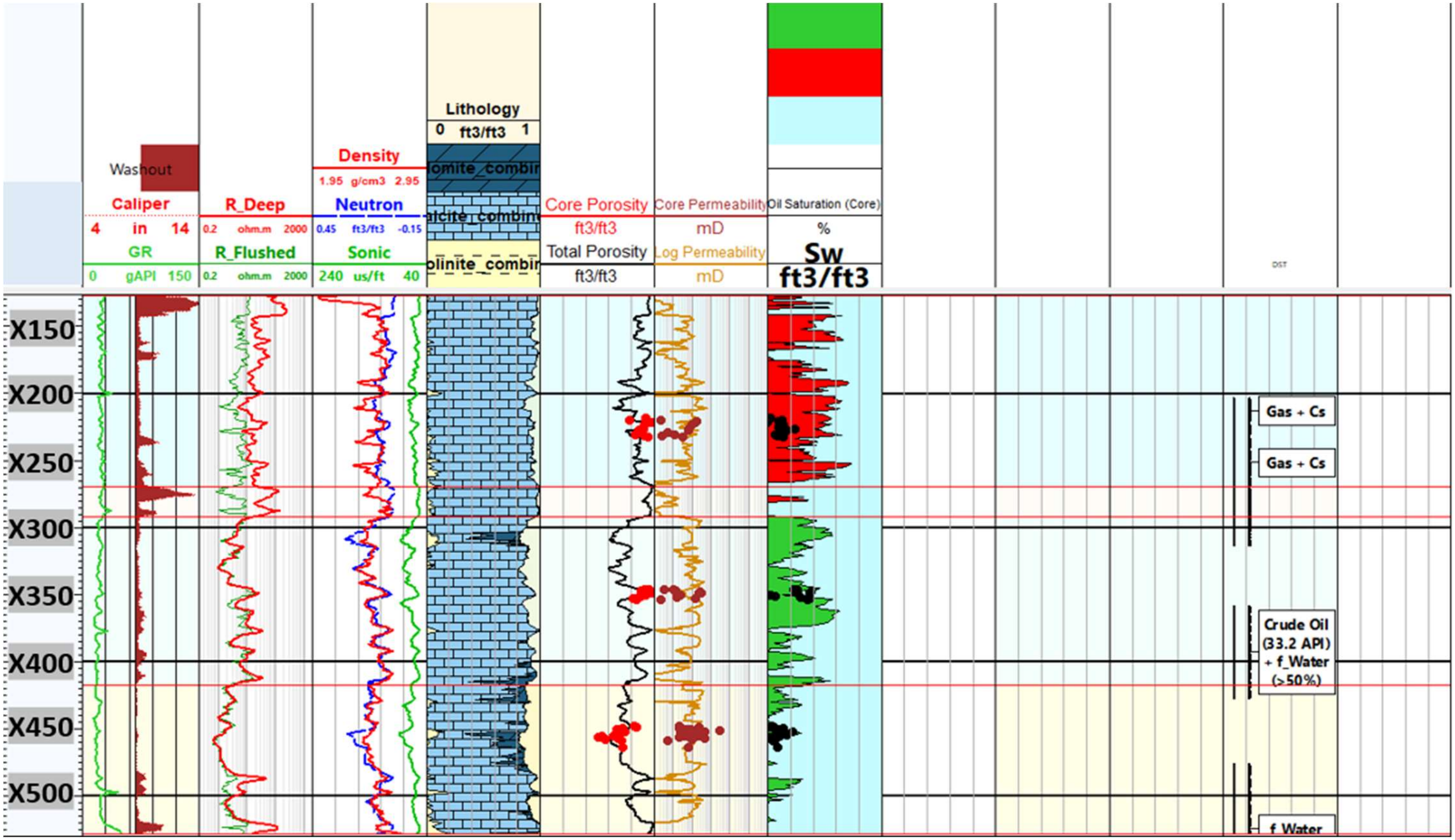

Figure 6. The plot shows available log data in well C. The gas-oil contact is defined based on the flushed and deep resistivity separation and DST.

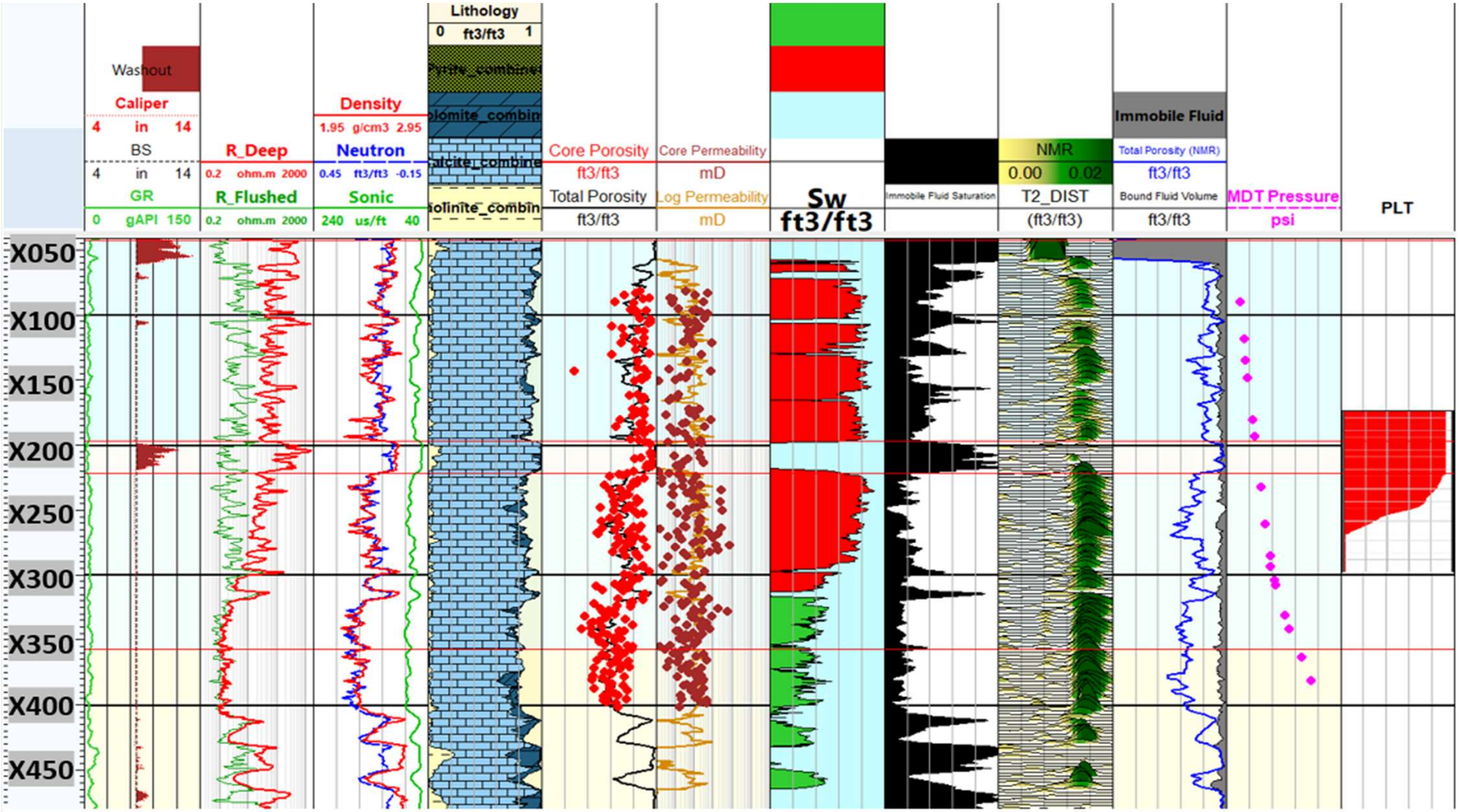

Figure 7. The plot shows available log data in well D. The gas-oil contact is defined based on the flushed and deep resistivity separation and pressure gradient data. There is a notable increase of immobile fluid towards the upper part of the gas condensate reservoir.

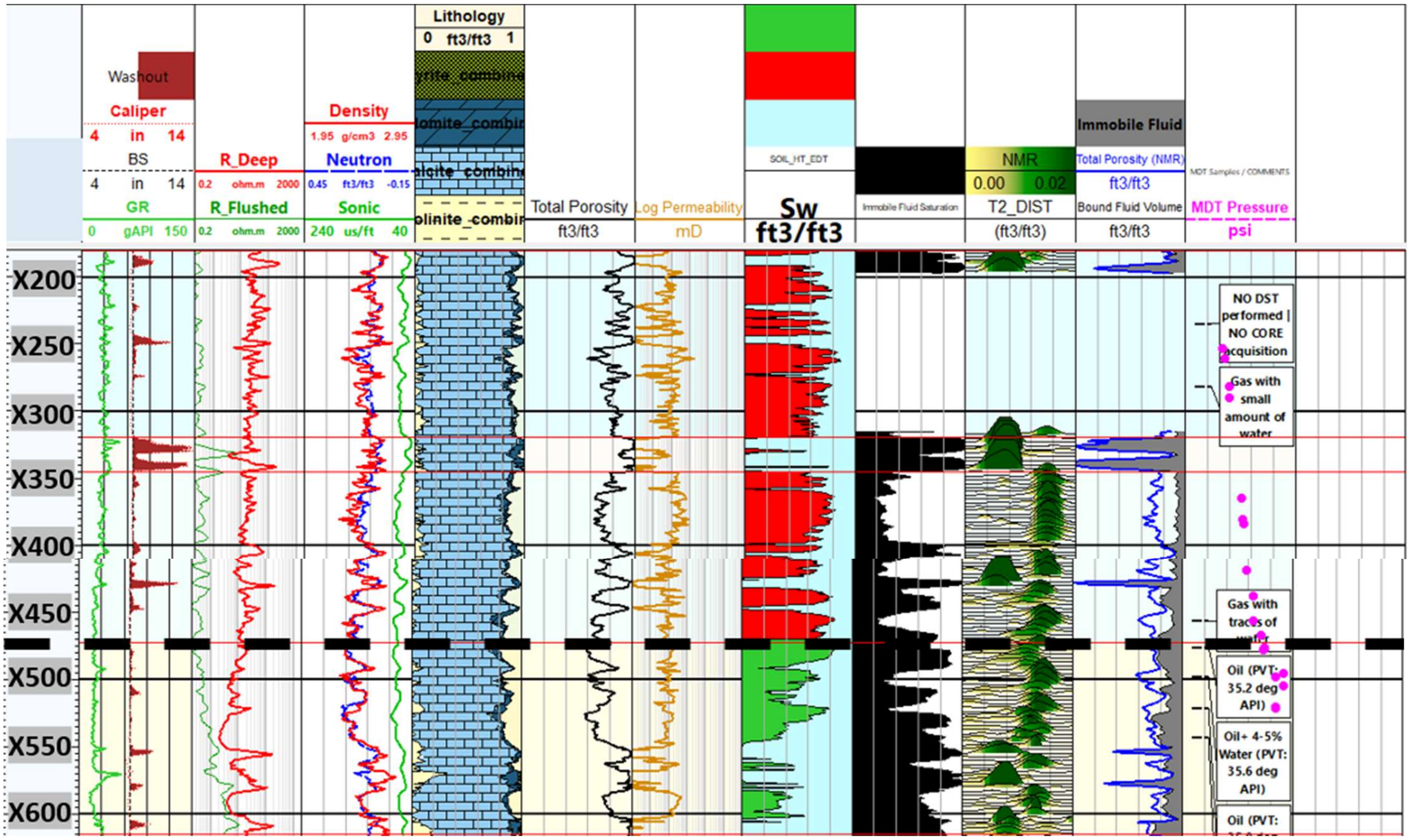

(a)

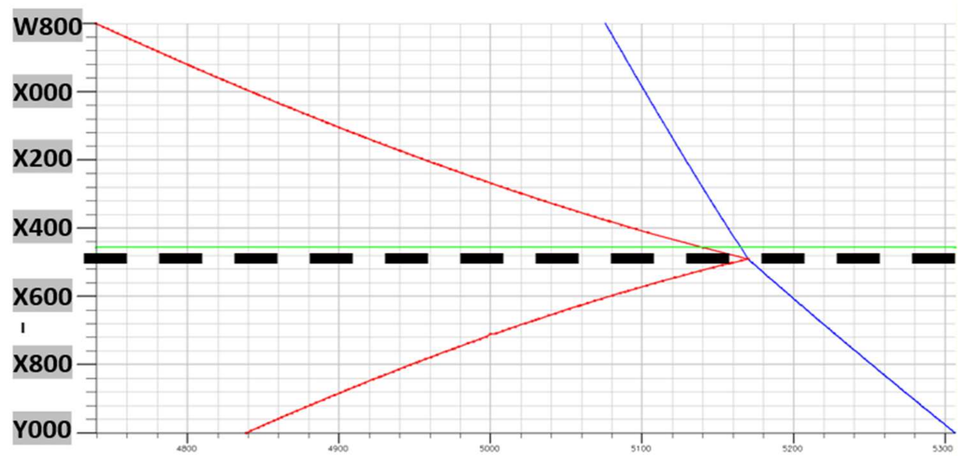

(b)

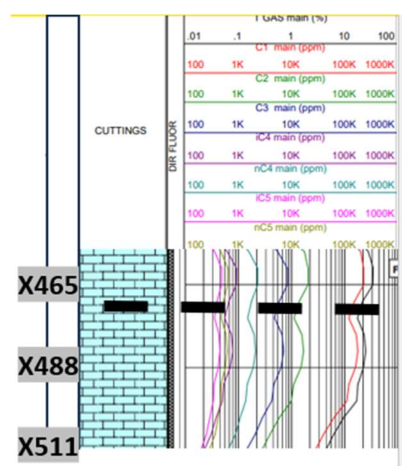

(c)

Figure 8. Available data of well E are shown here: (a) The possible gas-oil contact at around X470 is also marked by significant increase of irreducible fluid saturation from NMR towards the bottom of the reservoir; (b) Compositional grading simulation depicts the possible gas-oil contact at around X470; (c) Gas chromatogram shows downward decrease in gas reading from X470.

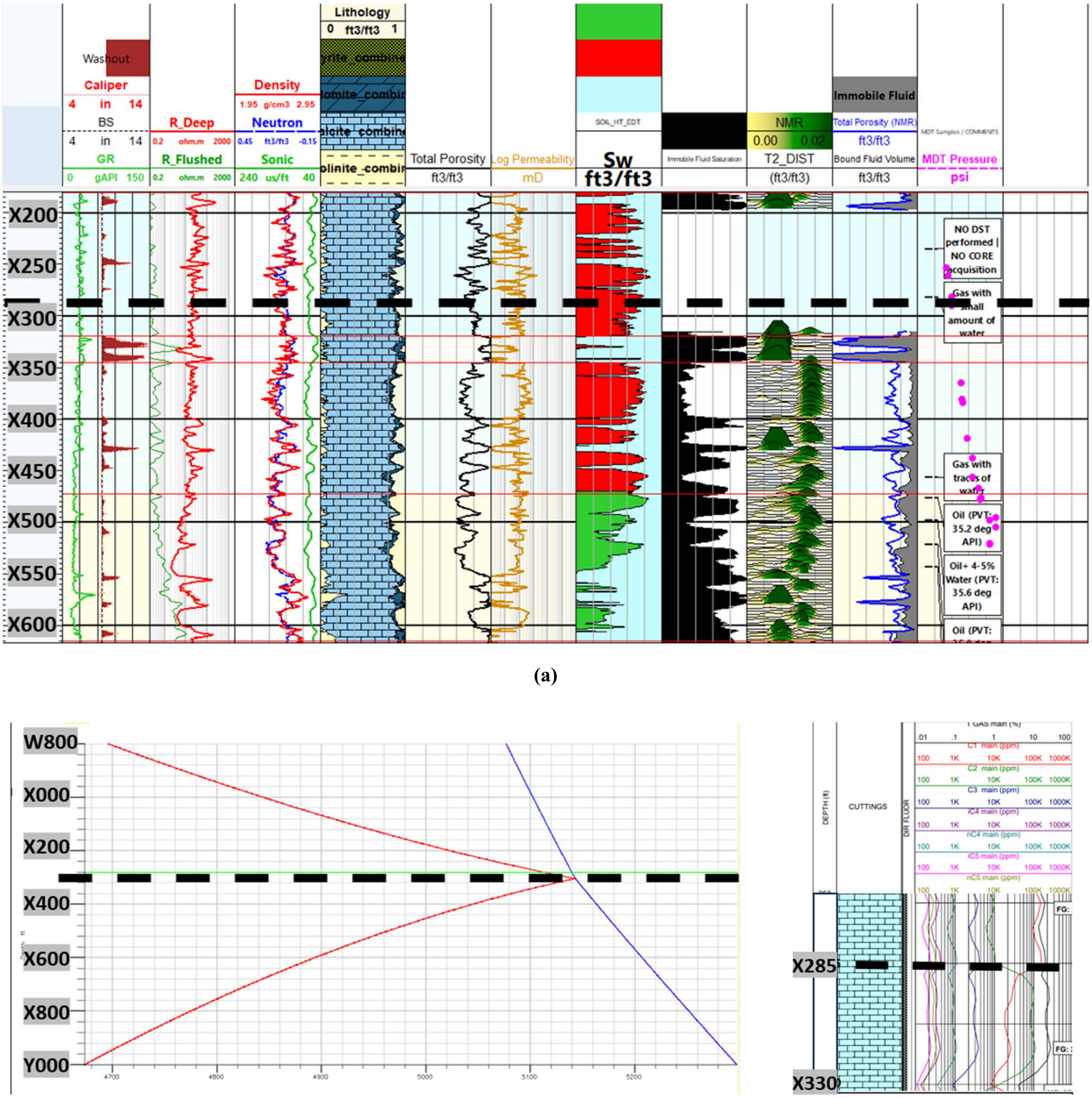

(a)

(b)

(c)

Figure 9. Available data of well E are shown here: (a) The possible gas-oil contact at around X285, where standard open-hole logs don't show any indication of fluid contact; (b) Compositional grading simulation depicts the possible gas-oil contact at around X285; (c) Gas chromatogram shows a significant decrease of C1 at around X285, creating a C1-C2 crossover.

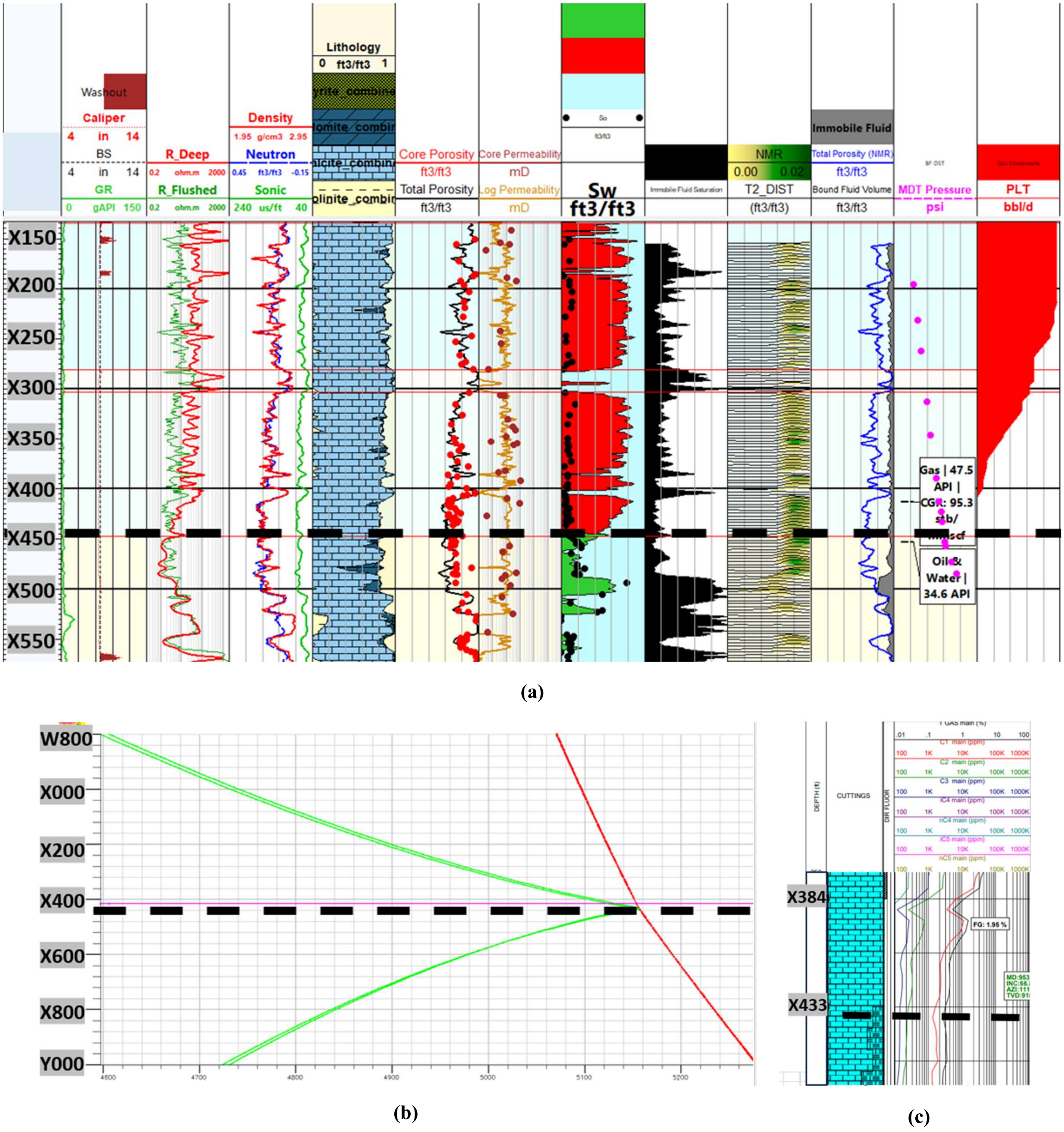

(a)

(b)

(c)

Figure 10. Available data of well E are shown here: (a) The possible gas-oil contact at around X445; (b) Compositional grading simulation depicts the possible gas-oil contact at around X445 (c) Gas chromatogram shows a significant decrease at around X445.

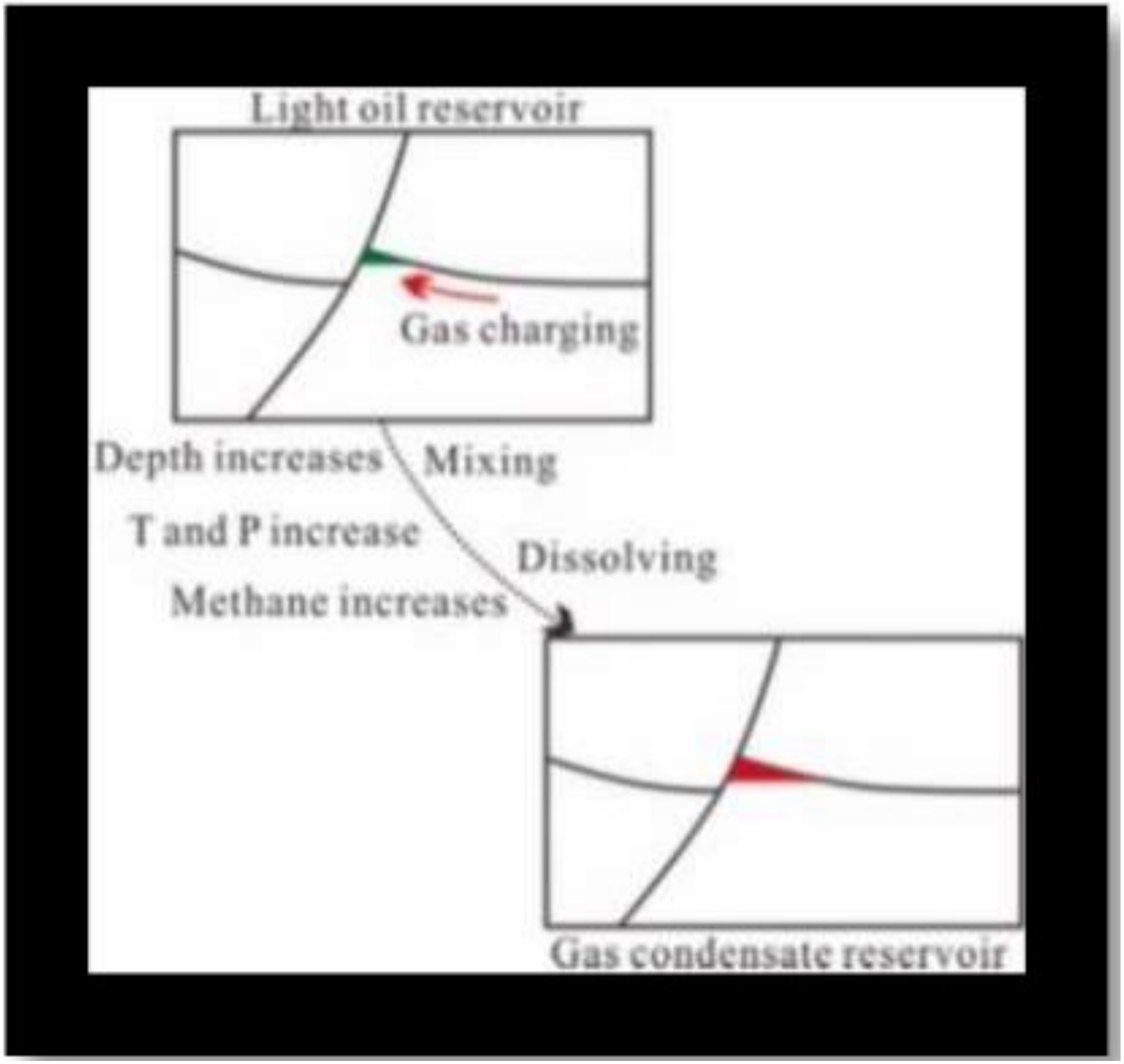

Figure 11. Illustration of the forming of gas condensate reservoir from light oil reservoir (Wang et al., 2022).

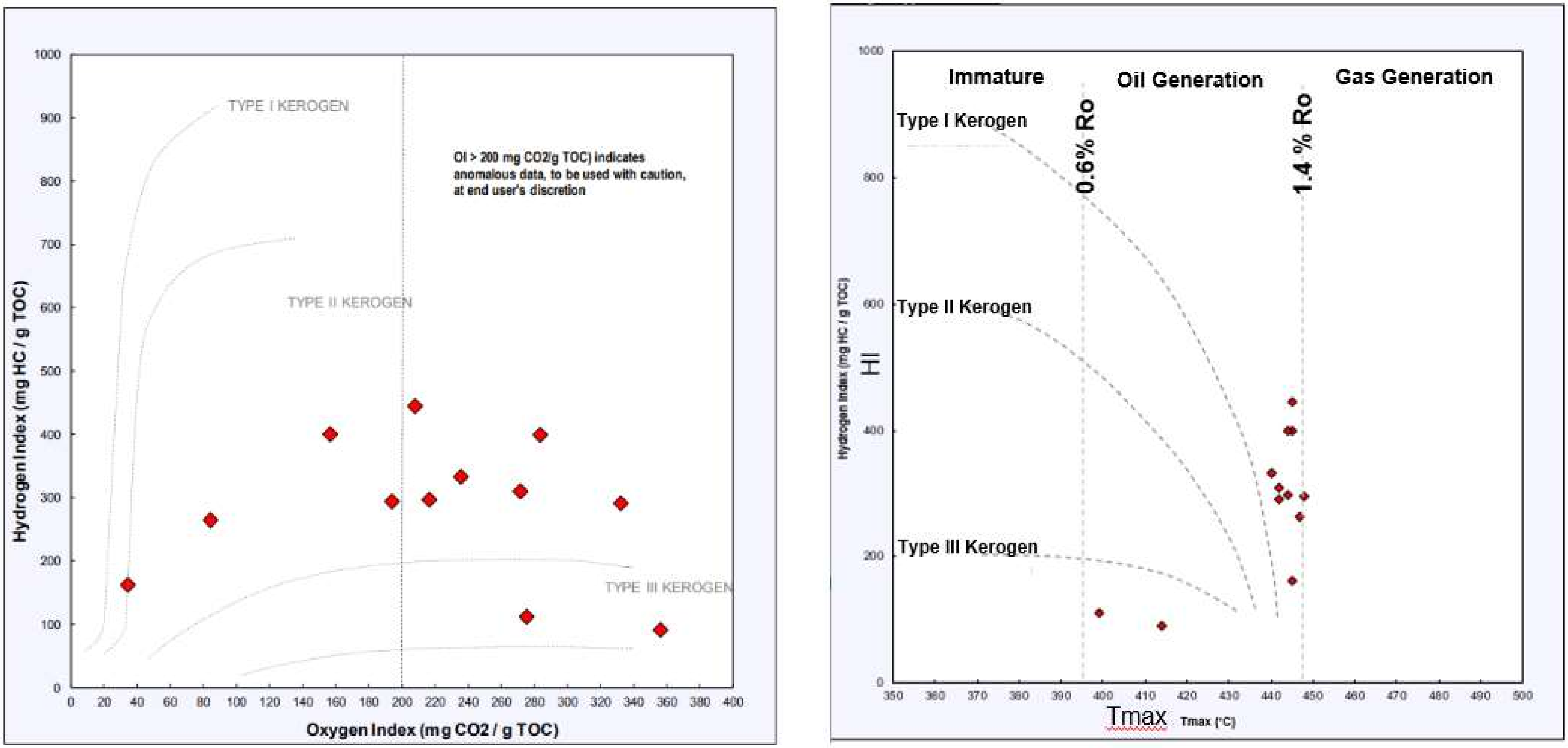

(a) (b)

Figure 12. Rock-eval pyrolysis shows the presence of oil prone type-II kerogen: (a) Modified van Krevelen diagram which utilizes oxygen index and hydrogen index shows type-II kerogen source rocks; (b) The plot of Tmax and hydrogen index shows the source rocks maturity within the oil generating window.

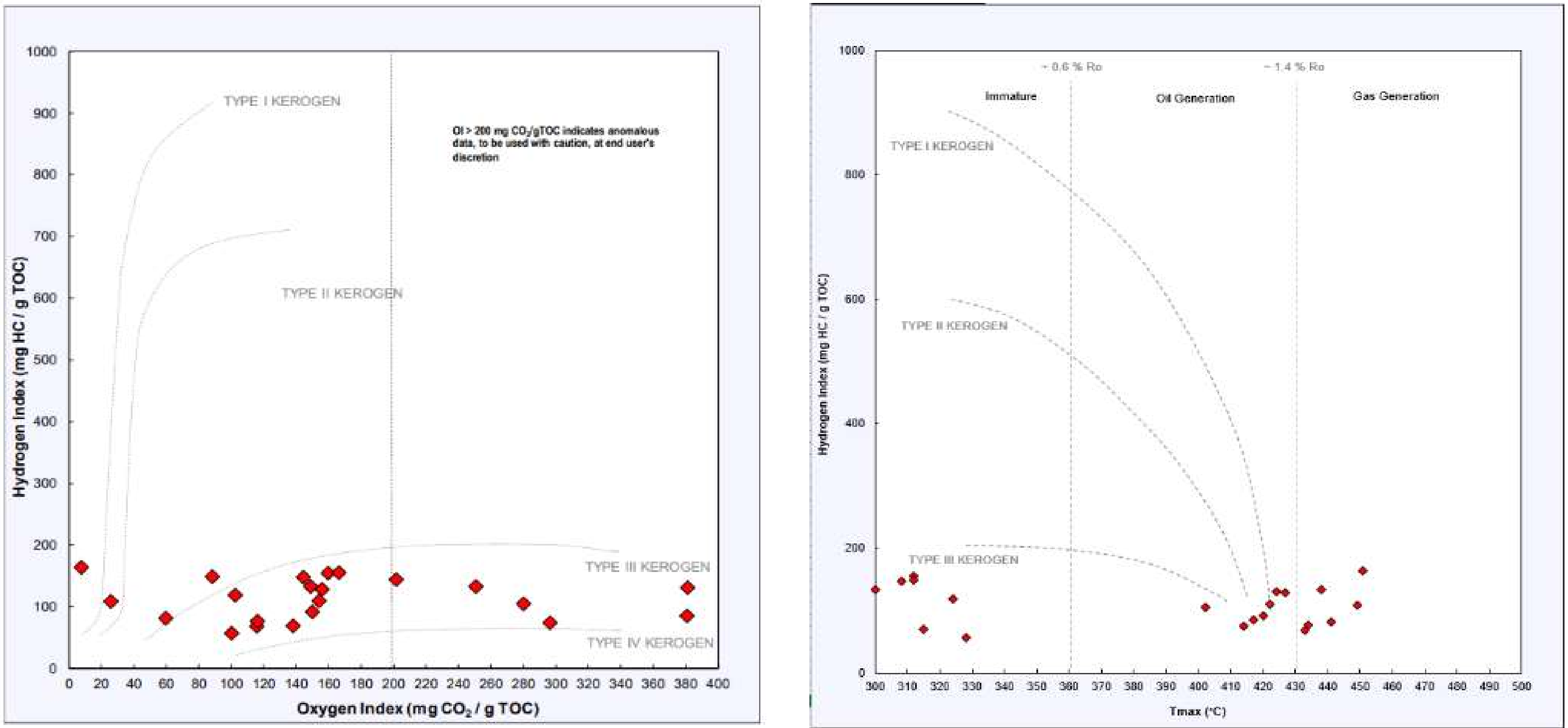

(a) (b)

Figure 13. Rock-eval pyrolysis shows the presence of gas prone type-III kerogen: (a) Modified van Krevelen diagram which utilizes oxygen index and hydrogen index shows type-III kerogen source rocks; (b) The plot of Tmax and hydrogen index shows the source rocks maturity reaching gas generating window.

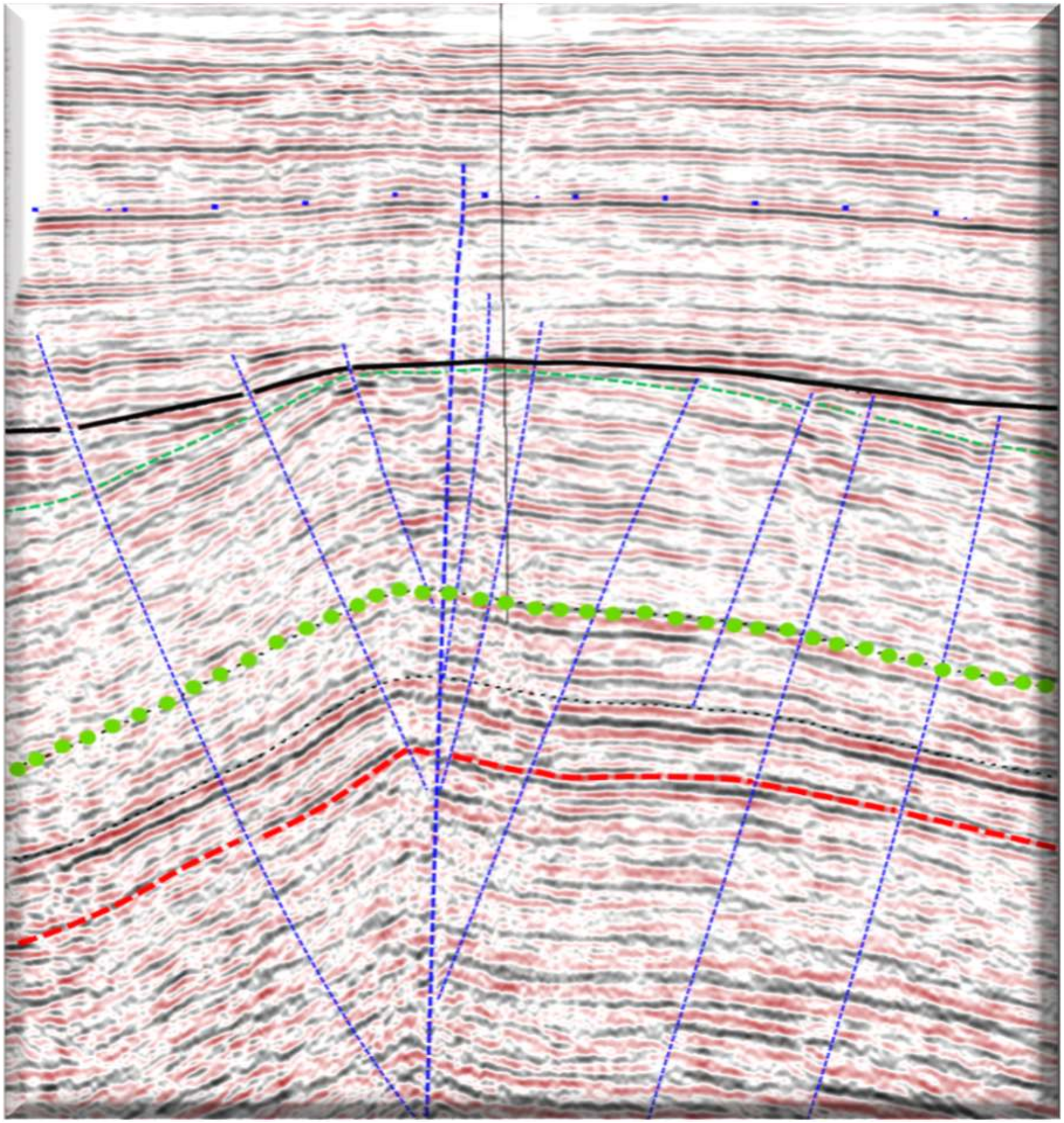

Figure 14. Seismic section shows developed flower structure in this field which favors the hydrocarbon migration from the source rock (red-dash line) to the reservoir (green-dotted line)